# Fiber cladding dual channel surface plasmon resonance sensor based on S-type fiber

Yong Wei(魏勇), Xiaoling Zhao(赵晓玲), Chunlan Liu(刘春兰)†, Rui Wang(王锐), Tianci Jiang(蒋天赐), Lingling Li(李玲玲), Chen Shi(石晨), Chunbiao Liu(刘纯彪), and Dong Zhu(竺栋)

*College of Electronic and Information Engineering, Chongqing Three Gorges University, Chongqing* 404100, *China*

(Received 16 March 2022; revised manuscript received 24 June 2022; accepted manuscript online 5 July 2022)

Fiber cladding surface plasmon resonance (SPR) sensors have few structures, and a clad SPR sensor based on S-type fiber is proposed in this paper. This new type of fiber cladding SPR sensor was formed by electrofusing an S-shaped structure on the fiber to couple the light in the fiber core to the cladding. In this paper, the effects of fiber parameters on the performance of the sensor were studied by simulation and experiment. Based on the conclusion that the smaller the core diameter is, the closer the working band of the SPR resonance is to long wavelengths, and that the geometric characteristics mean that a multimode fiber can receive the fiber cladding light from a small core diameter few-mode fiber, a dual channel SPR sensor with a double S-type fiber cascade was proposed. In the refractive index detection range of 1.333–1.385 refractive index units (RIU), the resonant working band of channel I is 627.66 nm–759.78 nm, with an average sensitivity of 2540.77 nm/RIU, and the resonant working band of channel II is 518.24 nm–658.2 nm, with an average sensitivity of 2691.54 nm/RIU. The processing method for the S-type fiber cladding SPR sensor is simple, effectively solving the problem of this type of SPR sensor structure and the difficult realization of a dual channel. The sensor is expected to be used in the fields of medical treatment and biological analysis.

**Keywords:** surface plasmon resonance (SPR), S-type structure, dual channel, cladding fiber SPR sensor

**PACS:** 07.07.Df, 42.81.Cn, 71.45.Gm **DOI:** 10.1088/1674-1056/ac7e3b

## 1. Introduction

Fiber surface plasmon resonance (SPR) sensors have the advantages of high sensitivity, good integration[1,2] and label-free and real-time online monitoring,[3,4] and have been widely used in the fields of chemical reaction and detection of biomolecular analyte reactions.[5–7] The occurrence of SPR on an optical fiber requires the evanescent field of transmitted light in the optical fiber to contact with the metal film, so that the evanescent wave can resonate with the surface plasma wave of the metal film. According to the position of the fiber substrate where SPR occurs, fiber SPR sensors can be divided into core type and cladding type. Core-type SPR sensors have the core exposed by removing the optical fiber cladding, and a metal film is plated on the surface of the exposed core to make the evanescent field of the core mode contact with the metal film, thus producing SPR. Typical methods for removing cladding and constructing an SPR optical fiber sensing structure include the side throwing method,[8,9] the grinding method,[10–12] and the corrosion method.[13–16] These processing methods often require complex microprocessing equipment, with problems such as low processing efficiency and the sensing probe being easily damaged. In recent years, fiber-clad SPR sensors have become a new research hotspot.

A fiber cladding SPR sensor couples the light transmitted in the fiber core to the cladding, and a metal film is plated on the cladding surface. The evanescent field of the cladding mode contacts the metal film to produce SPR. A typical fiber cladding SPR sensor is a heterocore structure composed of a multimode fiber, a single-mode fiber and a multimode fiber.[17–19] By the method of core mismatch, the light in the core of the multimode fiber is directly coupled and injected into the cladding of the single-mode fiber, and then a metal film is plated on the cladding of the single-mode fiber. This fiber cladding SPR sensor can be fabricated just by simple welding, with simple processing, low cost and a strong probe structure. However, there are few reported fiber cladding SPR sensor structures because there are few structures that can effectively couple the light in the fiber core to the cladding to construct such a sensor.

In this paper, we propose and demonstrate a novel fiber cladding SPR sensor based on an S-type fiber structure. Due to the S-type fiber structure, the light in the fiber core is coupled to the fiber cladding. By directly coating a 50 nm gold film outside the fiber cladding and splicing a multimode fiber with a larger core diameter to receive the cladding light, a fiber cladding SPR sensor was realized. Further, the effects of different kinds of S-type fibers and S-type fibers with different core diameters on the performance of the SPR sensor were also studied. The results indicate that, for few-mode step index S-type fibers, the smaller the core diameter is the closer the corresponding SPR resonance working band is to longer wavelengths.

A fiber cladding SPR dual channel sensor based on wave-

†Corresponding author. E-mail: lclliuchunlan@163.com

© 2023 Chinese Physical Society and IOP Publishing Ltd 

length division multiplexing technology requires two sensing areas with inconsistent SPR working bands on the same fiber.[20–23] By employing the structural characteristics that (i) the working band of the few-mode fiber cladding SPR sensor based on S-type fiber with a thin core diameter is closer to long wavelengths, (ii) the working band of the multimode fiber cladding SPR sensor based on S-type fiber with a thick core diameter is closer to short wavelengths, and (iii) the multimode fiber can receive the light from the cladding of the few-mode fiber, a dual-channel SPR sensor with double S-type fiber cascade is constructed that effectively solves the difficulty of dual-channel realization of a fiber SPR sensor.

## 2. Sensing principles and probe fabrication

### 2.1. Study of the cladding mode excitation of S-type fiber

In order to study the characteristics of the S-type fiber coupling the light in the core to the cladding, the light transmission characteristics of single-mode straight fiber and single-mode S-type fiber were simulated by Rsoft software. The simulation results for the beam transmission path are shown in Figs. 1(a) and 1(e), and the energy monitoring diagram of the fiber cladding is shown in Figs. 1(b) and 1(f). The diameter and refractive index of the single-mode fiber core and cladding are 9 μm and 125 μm and 1.457 and 1.4468, respectively. The length of the fiber is 950 μm, the length of the S-type structure is 350 μm and its vertical axis offset $\Delta x$ is 60 μm. As shown in Figs. 1(a), 1(b), 1(e), and 1(f), the single-mode straight fiber maintains stable transmission of the light in the core and the single-mode S-type fiber couples the light in the core to the cladding.

Next, experimental verification of the optical transmission characteristics of the S-type fiber was carried out. Figures 1(c) and 1(d) show micrographs of the side transmission light field and end exit light field, respectively, of a single-mode straight fiber, and figures 1(g) and 1(h) show micrographs of the side transmission light field and end exit light field, respectively, of a single-mode S-type fiber. It can be clearly seen from the figure that the light only propagates along the fiber core in the single-mode straight fiber. However, when we fabricate an S-type structure on the single-mode fiber, the cladding mode is excited when the transmission light passes though the S-type structure, which provides a structural basis for the construction of an S-type fiber cladding SPR sensor. Simulation and verification experiments indicate that the vertical axis offset is too small to effectively couple the light in the single-mode fiber to the cladding. If the vertical axis offset is too large, the light will leak out of the cladding and be lost. When the vertical offset is 60 μm, the efficiency of optical coupling to the cladding in the fiber core is high, and the cladding mode can be stably transmitted. In this paper, a vertical axis offset $\Delta x = 60$ μm was selected to conduct the follow-up experiments.

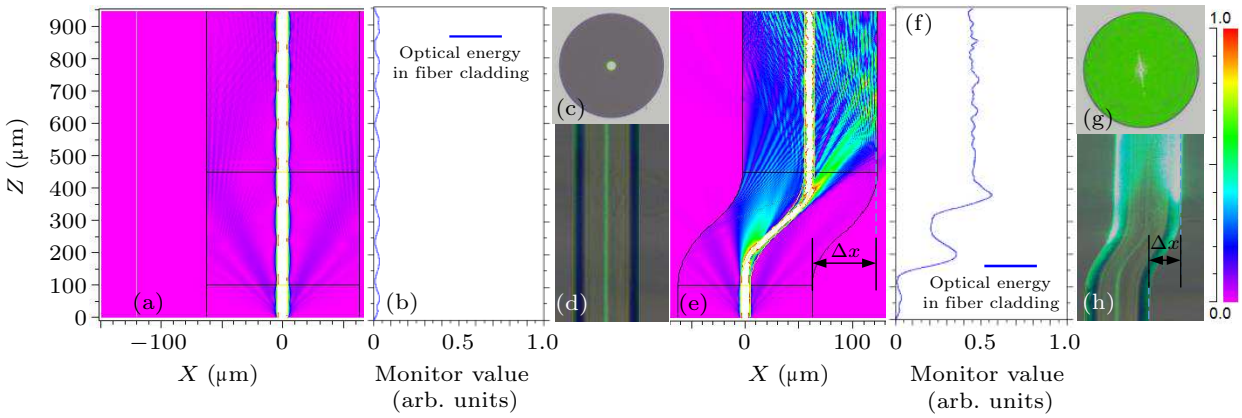



**Fig. 1.** (a) Simulation diagram of a single-mode straight fiber. (b) Light energy curve of single-mode straight fiber cladding. (c) Experimental micrograph of the end light field of a single-mode straight fiber. (d) Experimental micrograph of the side light field of a single-mode straight fiber. (e) Simulation diagram of a single-mode S-type fiber. (f) Light energy curve of single-mode S-shaped fiber cladding. (g) Experimental micrograph of the end light field of a single-mode S-type fiber. (h) Experimental micrograph of the side light field of a single-mode S-type fiber.

### 2.2. Structure and fabrication of an S-type fiber cladding SPR probe

According to the excitation characteristics of the S-type fiber cladding mode, we designed and constructed a cladding SPR sensor based on S-type fiber. The structural diagram is shown in Fig. 2(a). The probe consists of a thin core sensing fiber and a thick core receiving fiber. An S-shaped structure was prepared on the sensing fiber, and the SPR sensing area was prepared in the 2 cm cladding area behind the S-shaped structure. The broad-spectrum light source was injected from the left side of the sensing fiber. When passing through the S-shaped area, most of the light transmitted in the fiber core is coupled to the cladding. The evanescent field of the cladding mode contacts the 50 nm gold film on the cladding surface to produce SPR, and the cladding light is injected into the fiber core of the thick core receiving fiber. Figure 2(b) shows an electron micrograph of the S-type fiber cladding SPR sensing

probe.

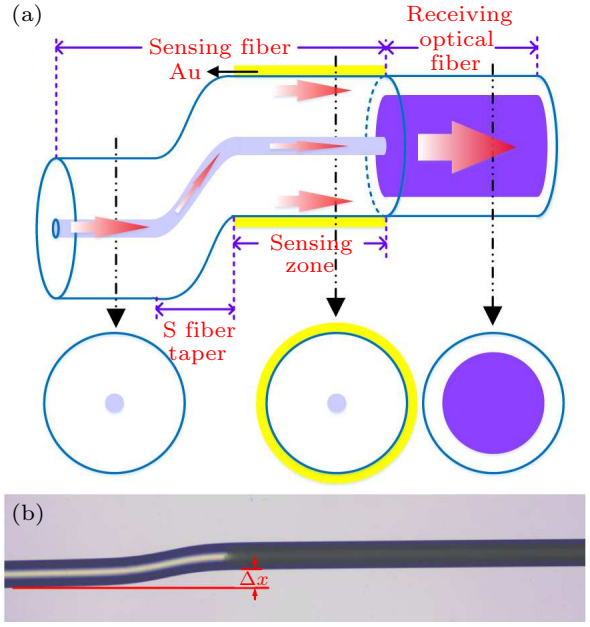



**Fig. 2.** (a) Schematic diagram of the S-type fiber cladding SPR sensing probe and (b) electron micrograph.

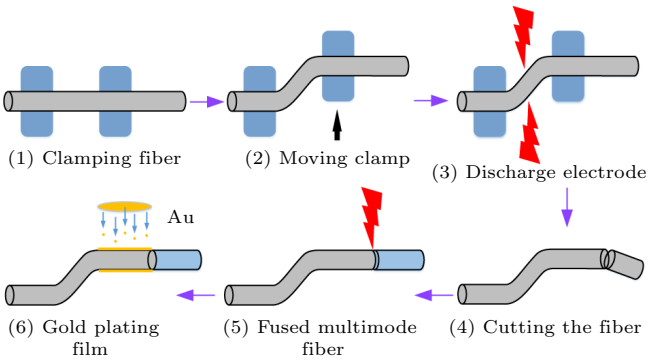



**Fig. 3.** Preparation process for the S-type fiber cladding SPR sensing probe.

The process for preparation of an S-type fiber cladding SPR sensing probe is shown in Fig. 3. We first employed a single-mode fiber (SMF-28e, Corning) to fabricate the sensing fiber. Using Miller pliers, the right side coating film of the single-mode fiber with a length of 5 cm was peeled off. The two ends of the single-mode fiber without coating film were clamped in the left and right clamps of an optical fiber welding machine (FL-116, FiberLink). Using the manual mode of the welding machine, the relative position of the two fiber clamps on the $y$-axis was adjusted to produce a vertical axis offset along the $y$-axis direction, and the fiber became S-shaped under the action of the vertical axis offset thrust. Controlling the welding machine to discharge, the pre melting time and welding time were set to 0.05 s and 0.8 s, respectively, the pre melting power and welding power were set to 70 W and 75 W, respectively, and the $x$-axis propulsion of the two fixture motors of the welding machine was set to 0. Under the action of vertical axis offset thrust and high-temperature discharge heating, the optical fiber was bent into an S-shape. The horizontal length of the S-type fiber area was 350 μm and the vertical axis offset was 60 μm. A fixed length cut was made at 2 cm on the right side of the S-shaped area and the end face of the optical fiber was cut flat. A thick core step index multimode fiber (SI105/125-22/250, YOFC) was used as the light receiving fiber. After the left end face was cut flat, the thick core multimode fiber was welded with the right end of the prepared S-type single-mode fiber. The fabricated fiber probe was placed in a magnetron sputtering instrument (ETD-650MS, Vision Precision Instruments) so that the 2 cm cladding area behind the S-type area of the sensing single-mode fiber was directly below the gold target, and the 50 nm gold film was coated outside the fiber cladding. Study of S-type clad SPR sensors with different gold film thickness has shown that a sensor with a 50 nm thick gold film has high average sensitivity and the deepest resonance valley. Thus the single-mode S-type optical fiber cladding SPR sensing probe was finished.

## 3. Experiments and results

### 3.1. Construction of the experimental device

The fiber cladding SPR refractive index sensing test system is shown in Fig. 4. The light emitted by the broad-spectrum light source (HL-2000, Ocean Optics) was injected into the left side of the sensing fiber and coupled into the cladding of the sensing area after the S-shaped structure of the sensing fiber. The evanescent field of the cladding mode contacted the gold film on the surface of the sensing area to produce SPR. The light receiving thick core fiber received the cladding light after SPR, sent it to the spectrometer (USB2000+, Ocean Optics) to collect data and then sent it to the computer for data processing. The sensing area of the S-type fiber cladding SPR sensor was sealed in the reaction reservoir. Standard testing solutions with different refractive indices were injected into the reaction reservoir through the micro flow pump, and the tested solution was discharged into the waste reservoir.

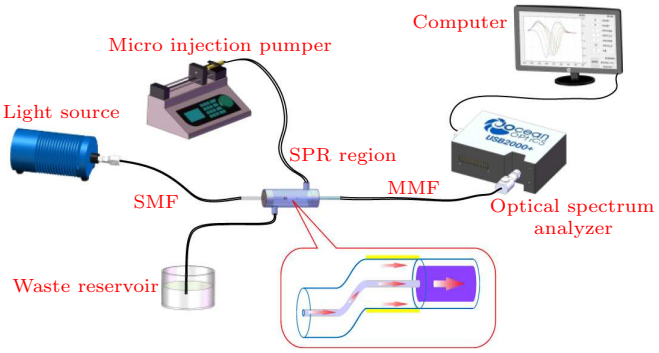



**Fig. 4.** Schematic diagram of fiber cladding SPR refractive index sensing testing system.

### 3.2. Experimental results

As shown in Fig. 5, the single-mode S-type fiber cladding SPR sensor was experimentally tested within the refractive index testing range of 1.333–1.385 refractive index units (RIU). The test results indicate that, with increase in the solution refractive index, the wavelength of the SPR resonance valley moves to a longer wavelength, from 606.27 nm to 729.55 nm, proving that the S-type fiber cladding SPR sensor proposed in this paper can stably realize refractive index sensing. Figure 5(b) shows the SPR resonance valley wavelength for solutions with different refractive indices; the curve shows a good linearity and the average detection sensitivity is 2370.77 nm/RIU.

For S-type fibers with different core diameters, the ability to couple core modes into cladding modes and the coupled cladding modes will be different. Different cladding modes will affect the resonant band, sensitivity and other aspects of sensing performance of the fiber cladding SPR sensor. In order to study the influence of core diameter on the performance of the S-type optical fiber cladding SPR sensor we studied it by simulation and experiment. As shown in Fig. 6, we simulated the light transmission characteristics of S-type fibers with different core diameters using Rsoft. The total length of the optical fiber is 5 mm, the length of the S-shaped structure is 350 μm and the vertical axis offset is 60 μm. Figures 6(a)–6(c) show the simulation results for step index few-mode fibers with core diameters of 4.7 μm, 9 μm, and 19 μm, respectively. Figures 6(d) and 6(e) show the simulation results for step index multimode fibers with core diameters of 50 μm and 60 μm, respectively. Figures 6(f) and 6(g) show the simulation results for graded-index multimode fibers with core diameters of 50 μm and 62.5 μm, respectively. The simulation results indicate that the cladding modes excited by S-type fibers with different core diameters are different, which will affect the sensing performance of the fiber cladding SPR sensor, such as resonance band, sensitivity and so on. In the optical energy curve for the fiber cladding, the closer the value of the blue curve is to 1, the more optical energy there is optically coupled to the fiber cladding.

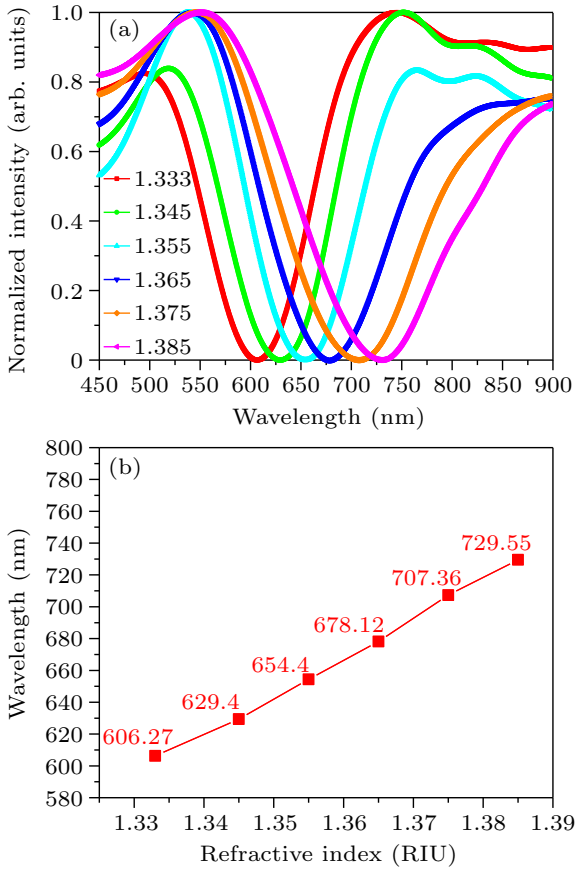



**Fig. 5.** Refractive index measurement results of the single-mode S-type fiber cladding SPR sensor: (a) experimental spectra; (b) the relationship between the refractive index and SPR resonance wavelength.

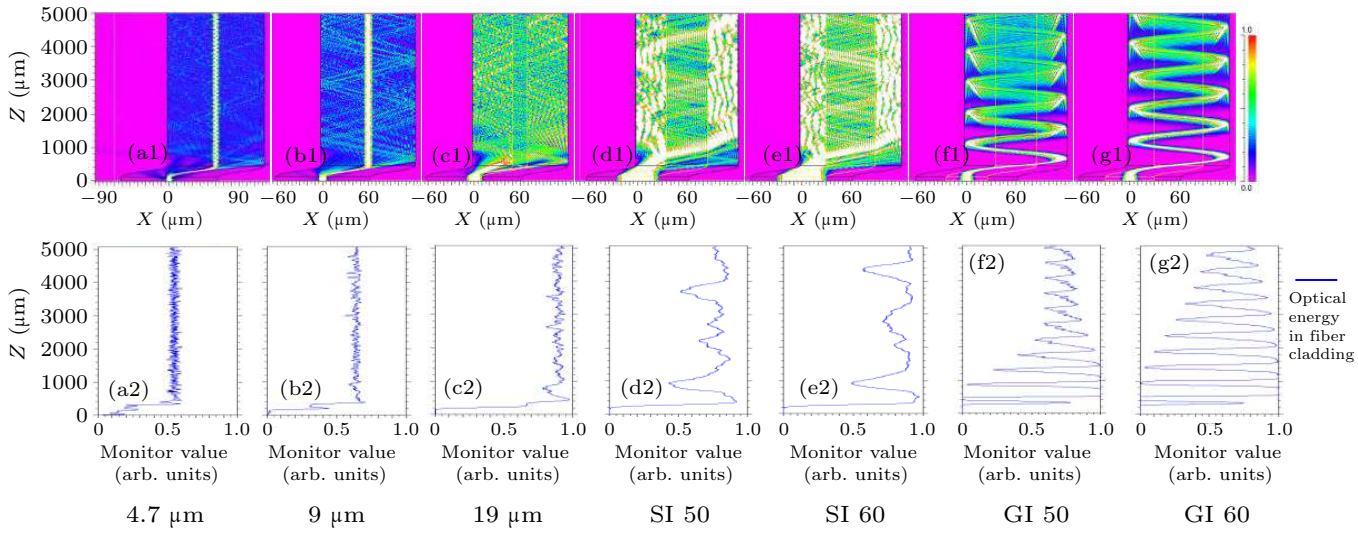



**Fig. 6.** Transmission characteristics: simulated results and optical energy curve of S-type few-mode fibers with different core diameters ((a) 4.7 μm, (b) 9 μm, (c) 19 μm), step-index multimode fibers with core diameters of (d) 50 μm and (e) 60 μm and graded-index multimode fibers with core diameters of (f) 50 μm and (g) 60 μm.

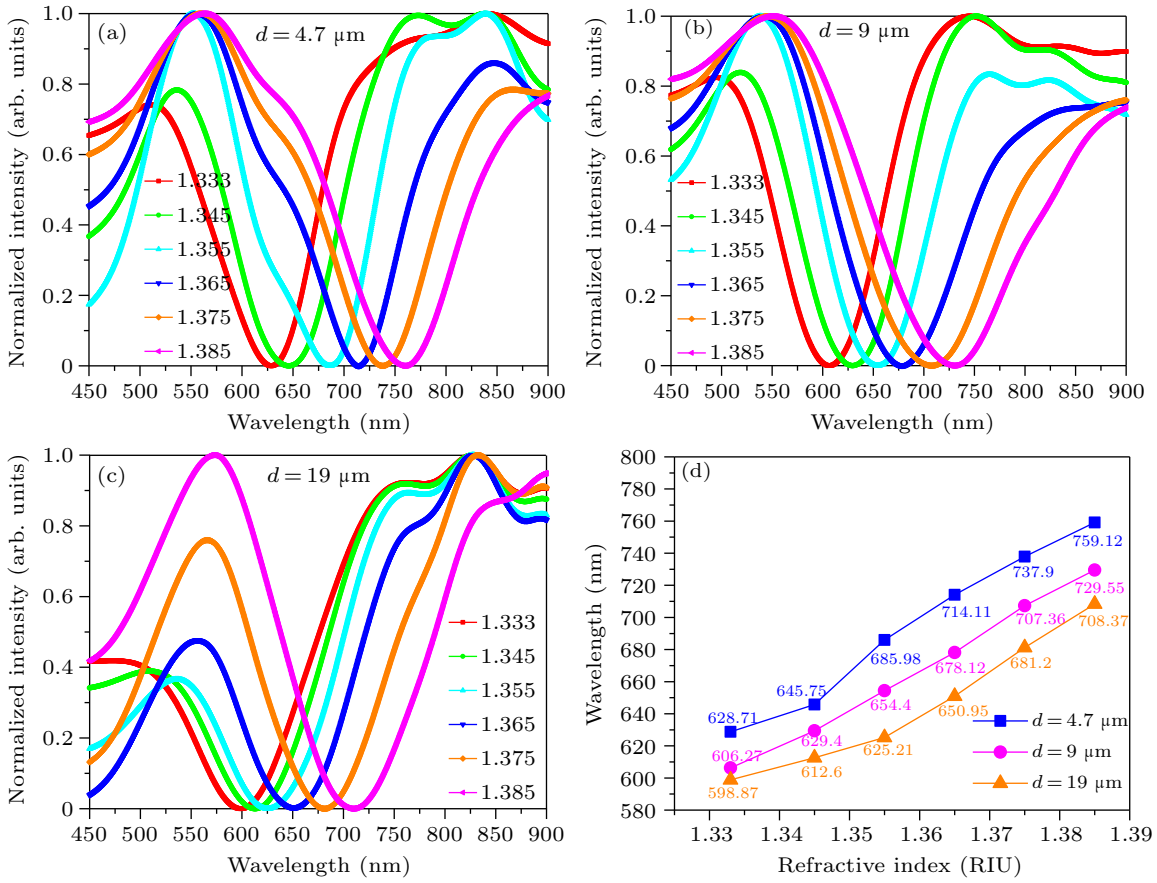



**Fig. 7.** Test results for few-mode S-type fiber cladding SPR sensors with core diameters of (a) 4.7 μm, (b) 9 μm, and (c) 19 μm. (d) The relationship between the refractive index of the solution and resonance wavelength.

In order to further study the influence of S-type fibers with different core diameters on the sensing performance, various S-type fiber cladding SPR sensors with different core diameters were fabricated and tested. Firstly, S-type few-mode fiber cladding SPR sensors with core diameters of 4.7 μm, 9 μm, and 19 μm were fabricated and tested. The test spectra of the SPR refractive index sensors are shown in Figs. 7(a)–7(c), and figure 7(d) shows the relationship between refractive index and resonance wavelength of the three sensors. From the test results, with increase in the refractive index of the solution, the SPR resonance wavelength moves to the long wavelength direction and the sensing can be well realized with the fiber cladding SPR sensor. When the fiber core is 4.7 μm, the resonance wavelength increases from 628.71 nm to 759.12 nm, and the average sensitivity is 2507.89 nm/RIU. When the fiber core is 9 μm and 19 μm, the dynamic range and sensitivity are 606.27 nm–729.55 nm and 598.87 nm–708.37 nm and 2370.77 nm/RIU and 2105.77 nm/RIU, respectively. The test results indicate that the smaller the core diameter of the few-mode step index S-type fiber is, the closer the SPR resonance working band is to the long wavelength and the higher the average sensitivity is.

Compared with few-mode fibers, the modes in multimode fibers are more complex. Multimode fibers include step index multimode fibers and graded-index multimode fibers. In order to specifically study the influence of fiber core diameter on the working performance of the sensor when the sensing fiber is a multimode fiber, we selected step-index multimode fibers and graded-index multimode fibers with core diameters of 50 μm and 60 μm and 50 μm and 62.5 μm, respectively, to fabricate the S-shaped fiber cladding SPR sensor and perform the refractive index sensing. The test results are shown in Fig. 8.

As shown in Figs. 8(a) and 8(b), when the sensing fiber is a step-index multimode fiber with a core diameter of 50 μm or 60 μm, the dynamic range and sensing sensitivity are 616.46 nm–724.52 nm and 603.45 nm–707.70 nm and 2078.08 nm/RIU and 2004.81 nm/RIU, respectively. As shown in Figs. 8(c) and 8(d), when the sensing fiber is a graded multimode fiber with a core diameter of 50 μm or 62.5 μm, the dynamic range and sensing sensitivity are 608.03 nm–722.18 nm and 591.44 nm–701.95 nm and 2195.19 nm/RIU and 2125.19 nm/RIU, respectively. Figure 8(e) shows the relationship between the refractive index of the four sensing probes and the SPR resonance wavelength. The test and calculation results indicate that when the sensing fiber is a multimode fiber, the larger the core diameter is the larger the half width and height of the SPR resonance valley is, and the worse the waveform of the resonance valley is the closer the working band of SPR resonance wavelength is to shorter wavelengths

and the lower the detection sensitivity, which is consistent with the law when the sensing fiber is a few-mode fiber. When the core diameter of multimode sensing fibers is the same, the average detection sensitivity of a graded-index multimode fiber is higher than that of a step index multimode fiber, and its resonant working band is closer to shorter wavelengths.

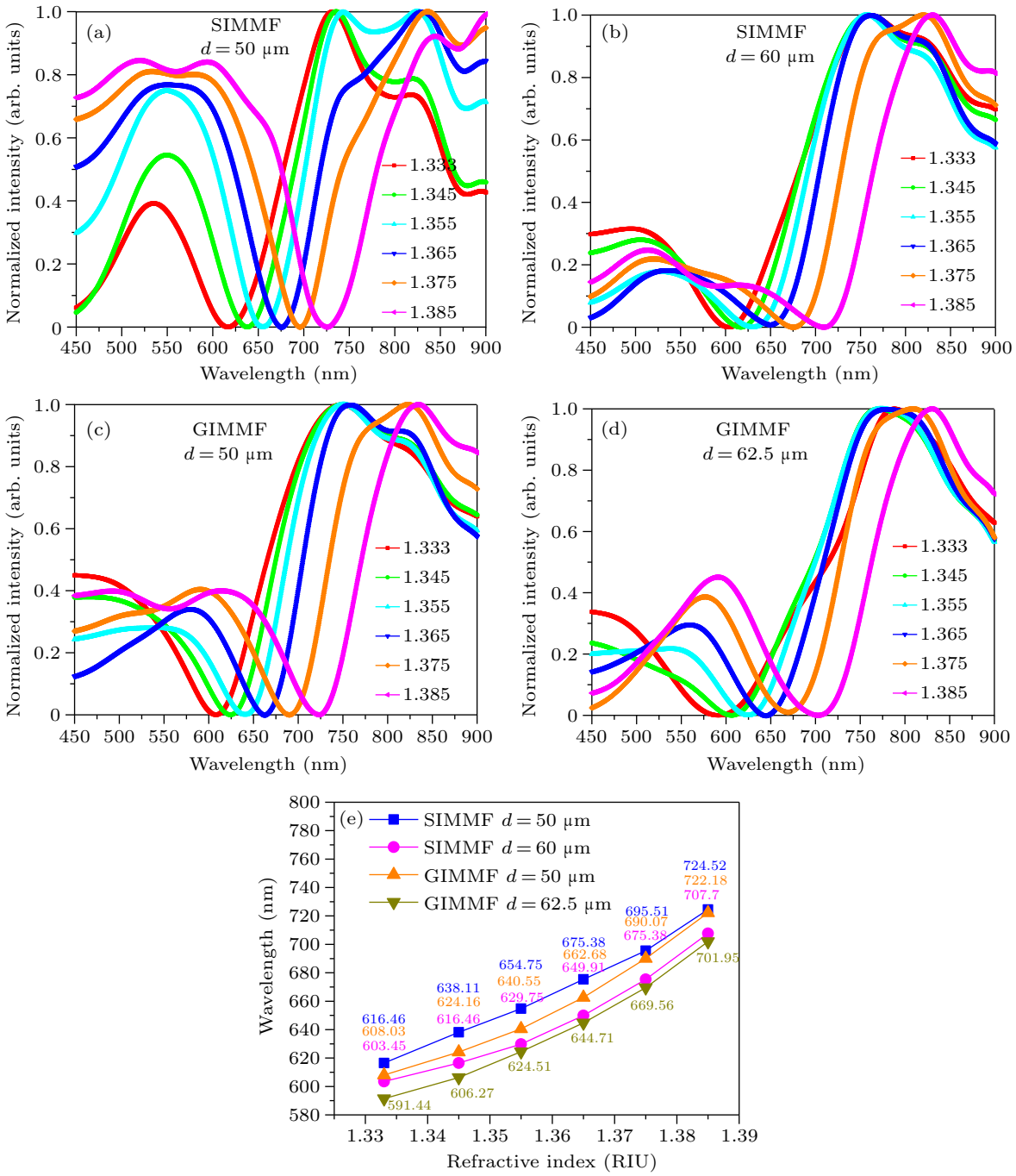



**Fig. 8.** Test results for multimode S-type fiber cladding SPR sensors: step-index multimode fiber with core diameters of (a) 50 μm and (b) 60 μm and graded-index multimode fiber with core diameters of (c) 50 μm and (d) 62.5 μm. (e) The relationship between the refractive index of the solution and resonance wavelength.

## 4. Discussion

For a fiber cladding SPR dual channel sensor based on wavelength division multiplexing technology it is necessary to construct two sensing areas with inconsistent dynamic range on the same fiber. Based on the research results above, the dynamic range of a few-mode fiber cladding SPR sensor is closer to the long wavelength direction, while that of a multimode fiber cladding SPR sensor is closer to the short wavelength direction. In addition, according to the geometric characteristics of the fiber, the partial cladding mode of a few-mode fiber with a small core diameter can be received by a multimode fiber with a large core diameter. For these reasons, we cascaded a few-mode fiber cladding S-type sensing probe with small core diameter and a multi-mode fiber cladding S-type sensing probe

with large core diameter to build an S-type fiber cladding SPR dual channel sensor, the structural diagram of which is shown in Fig. 9. We selected a few-mode fiber with a core diameter of 4.7 μm as channel I. This fiber has a dynamic range of 628.71 nm–759.12 nm which is closer to long wavelength direction. We selected a graded-index multimode fiber with a core diameter of 50 μm as channel II; its dynamic range is 608.03 nm–722.18 nm which is closer to the long wavelength direction and has a better spectral curve. In order to make the difference between the SPR resonance working bands of the two channels greater we introduced silver film to modify the second channel to move its SPR resonance working band closer to shorter wavelengths; the thickness of silver film was 50 nm. Compared with a sensing probe with 50 nm gold film, the dynamic range of the sensing probe with 50 nm silver film is wider, close to 100 nm. When the SPR resonance valleys of the silver and gold film appear at the same time they can be effectively separated. In addition, the core diameter of the S-type fiber cladding SPR sensor can be superimposed on the SPR resonance band and adjusted together, fully realizing the separation of two resonance valleys under one spectral scanning. Therefore, we selected gold and silver film thicknesses of 50 nm, which give the highest average sensitivity and the deepest resonance valley depth.

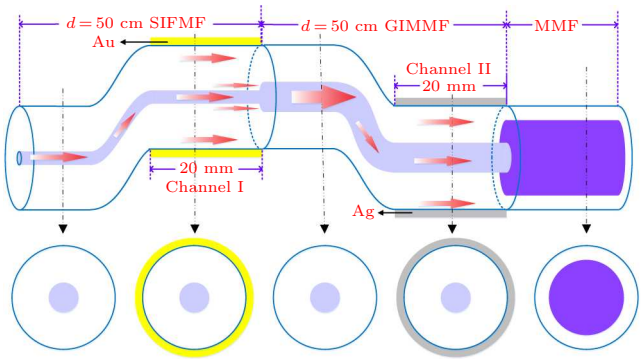



**Fig. 9.** Structure diagram of dual-channel SPR sensor with double S-type fiber cascade.

As shown in Fig. 9, the right end of the few-mode S-type SPR sensor with a core diameter of 4.7 μm (channel I) was spliced with the left end of a graded-index multimode fiber with a core diameter of 50 μm (channel II) to form a double S-type fiber cascade structure. A 50 nm gold film was coated on the 2 cm cladding surface behind the left S-shaped structure, and a 50 nm silver film was coated on the 2 cm cladding surface behind the right S-shaped structure, and testing of the refractive index sensing ability of the dual channel SPR was carried out.

Firstly, keeping channel II in the air, channel I was placed in the reaction reservoir and the testing solution with a refractive index of 1.333–1.385 was successively injected into the reaction reservoir; channel I then carried out refractive index sensing. As shown in Fig. 10(a), the resonance wavelength of SPR shifts from 639.85 nm to 781.12 nm, and the average sensitivity is 2716.73 nm/RIU. Similarly, we tested channel II. As shown in Fig. 10(b), when channel II works alone, due to the modification of silver film, its SPR resonance wavelength moves from 534.19 nm to 672.30 nm and the average sensitivity is 2655.96 nm/RIU. Compared with channel I, its dynamic range is closer to the shortwave length direction, and the difference between the working bands of the two channels can be more than 100 nm. When the channels work at the same time, the resonance valley can be effectively separated.

In order to study the refractive index response of two channels in solution at the same time, both channels were placed in the reaction reservoir, and the following experimental tests were carried out. First, a solution with a refractive index of 1.333–1.385 was successively injected into the reaction reservoir of channel I and distilled water with a refractive index of 1.333 was injected into the reaction reservoir of channel II. As shown in Fig. 11(a), the two resonance valleys of the two channels are well separated. The SPR resonance wavelength of channel I moves from 637.76 nm to 759.12 nm, which is basically consistent with the resonance band when channel I works alone. The SPR resonance valley of channel II stays still. Second, distilled water with a refractive index of 1.385 was injected into the reaction reservoir of channel I and the solution with a refractive index of 1.333–1.385 was successively injected into the reaction reservoir of channel II. As shown in Fig. 11(b), the two resonance valleys of the two channels are well separated. The SPR resonance wavelength of channel I stays still, and the SPR resonance wavelength of channel II moves from 522.23 nm to 658.20 nm, which is basically consistent with the resonance band when channel II works alone. Finally, the solution with a refractive index of 1.333–1.385 was successively injected into the reaction reservoirs of channels I and II at the same time. As shown Fig. 11(c), there are still two distinct SPR resonance valleys in the transmission spectrum. The SPR resonance wavelength of channel I moves from 627.66 nm to 759.78 nm, and the average sensitivity is 2540.77 nm/RIU. The SPR resonance wavelength of channel II moves from 518.24 nm to 658.20 nm, and the average detection sensitivity is 2691.54 nm/RIU. Which is basically consistent with the SPR resonance working band when the two channels work alone. Figure 11(d) shows the relationship between the refractive index of the solution to be measured and the resonance wavelength of the double S-type fiber cascaded dual channel sensor under different testing statuses. It can be seen from the figure that the SPR dynamic range of the two channels is basically consistent in various tests. Even in the case of the double S-type cascade, single channel independent operation and double channel simultaneous operation can be realized, and the refractive index result obtained with the SPR sensor is still accurate.

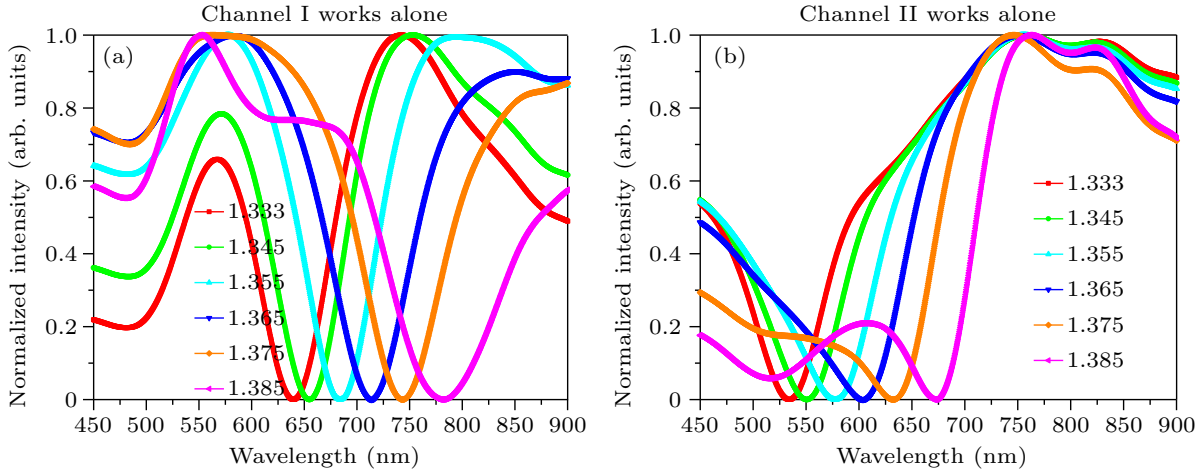



**Fig. 10.** Testing results for (a) channel I working alone and (b) channel II working alone.

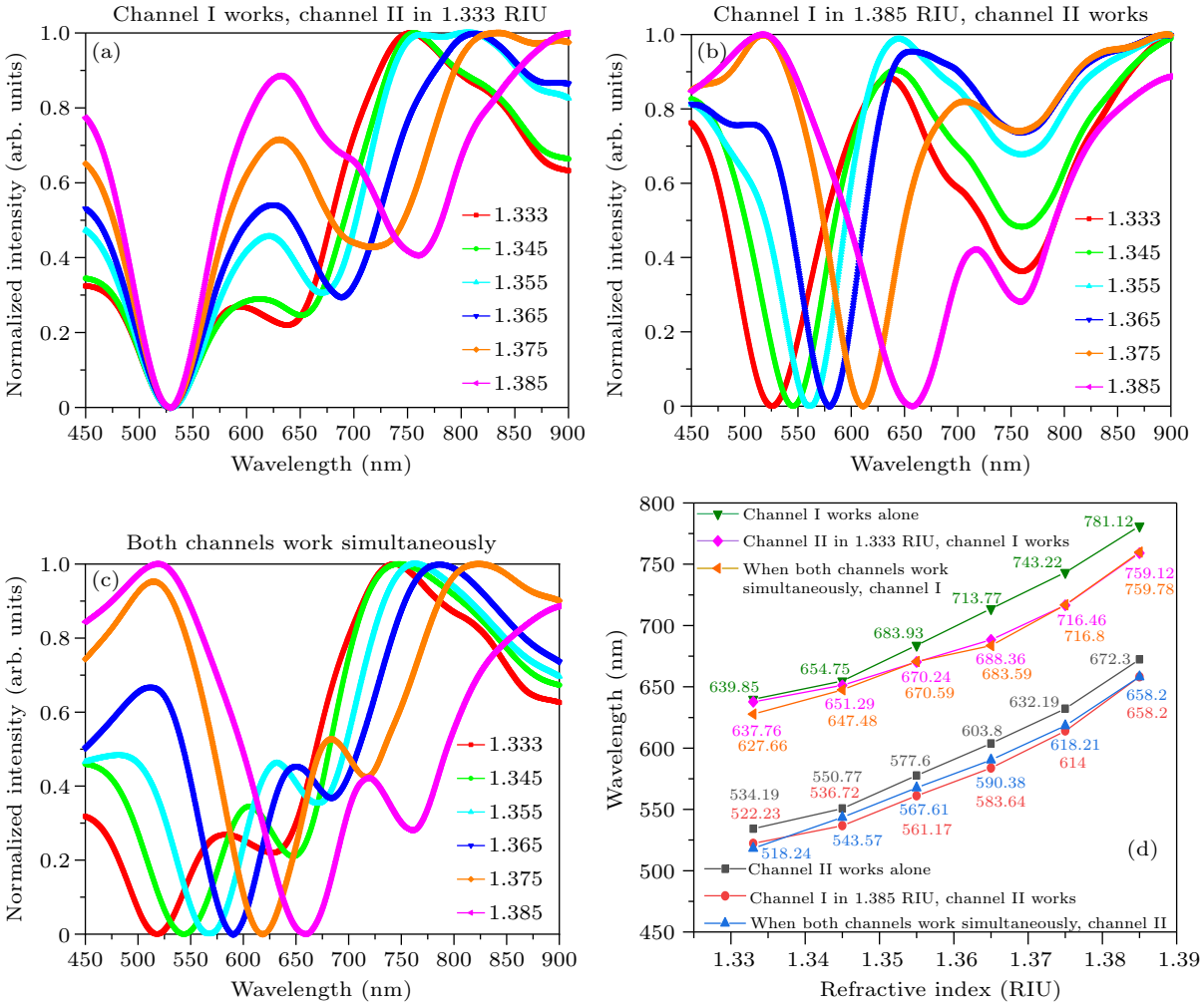



**Fig. 11.** Test results for a double S-type fiber cascaded dual-channel sensor with: (a) channel I in a solution with refractive index 1.333–1.385 and channel II in distilled water (refractive index 1.333), (b) channel I in solution with refractive index 1.385 and channel II in solution with refractive index 1.333–1.385 and (c) channel I and channel II both in solution with refractive index 1.333–1.385. (d) The relationship between the refractive index of the solution and resonance wavelength.

## 5. Conclusion

In this study, we proposed a novel S-type fiber cladding SPR sensor based on the characteristic that an S-type fiber can couple the light in the core to the cladding. By simulation and experiment, the influence of fiber core diameter on the SPR performance of the sensor was studied when the sensing fiber is a few-mode fiber, a multimode step-index fiber or a multimode graded-index fiber. The simulation and test results indicate that when the sensing fiber is a few-mode fiber the smaller the core diameter of the sensing fiber is, the closer the

dynamic range of SPR resonance is to a longer wavelength, and the higher the sensitivity is. The few-mode S-type fiber SPR sensor has the highest sensitivity of 2507.89 nm/RIU when the core diameter is 4.7 μm, and its dynamic range is 628.71 nm–759.12 nm. When the sensing fiber is a multimode fiber, the larger the core diameter is, the closer the dynamic range is to the shorter wavelength direction, while the half width height of the SPR resonance valley increases and the curve gradually deteriorates. Based on the characteristics that the dynamic range of an S-type fiber with a thick core is closer to the short wavelength direction while that of an S-type fiber with a thin core is closer to the long wavelength direction, and that the geometric characteristics that the fiber with a larger core diameter can receive the cladding mode of the fiber with a smaller core diameter, a dual channel SPR sensor based on cascaded double S-type fiber is constructed. The sensing fiber of channel I is a few-mode fiber with a core diameter of 4.7 μm, which has a dynamic range and sensitivity of 627.66 nm–759.78 nm and 2540.77 nm/RIU, respectively. The sensing fiber of channel II is a graded-index multimode fiber with a core diameter of 50 μm, which has a dynamic range and sensitivity of 518.24 nm–658.20 nm and 2691.54 nm/RIU, respectively. The proposed dual channel fiber SPR sensor based on an S-type structure solves the difficulties in implementation of fiber multi-channel sensors based on wavelength division multiplexing technology and is expected to be used in medical treatment, environmental monitoring, food safety detection and biomolecular analyte reaction detection.

## Acknowledgments

Project supported by the National Natural Science Foundation of China (Grant No. 61705025), Chongqing Natural Science Foundation (Grant Nos. cstc2019jcyj-msxmX0431 and cstc2018jcyjAX0817), the Science and Technology Project Affiliated to the Education Department of Chongqing Municipality (Grant Nos. KJQN201801217, KJQN201901226, KJQN202001214, and KJ1710247), Chongqing Key Laboratory of Geological Environment Monitoring and Disaster Early-Warning in Three Gorges Reservoir Area (Grant Nos. ZD2020A0103 and ZD2020A0102), and Fundamental Research Funds for Chongqing Three Gorges University of China (Grant No. 19ZDPY08).

## References

[1] Cao S Q, Shao Y, Wang Y, Wu T S, Zhang L F, Huang Y J, Zhang F, Liao C R, He J and Wang Y P 2018 *Opt. Express* **26** 3988
[2] Xia F, Song H, Zhao Y, Zhao W M, Wang Q, Wang X Z, Wang B T and Dai Z X 2020 *Measurement* **164** 108083
[3] Liu Y, Chen S M, Liu Q, Liu Z G and Wei P 2017 *Opt. Express* **25** 11750
[4] Primo E N, Kogan M J, Verdejo H E, Soledad B, Rubianes M and Rivas G A 2018 *ACS Appl. Mater. Interfaces* **10** 23501
[5] Shevchenko Y, Francis T J, Blair D A D, Walsh R, DeRosa M C and Albert J 2011 *Anal. Chem.* **83** 7027
[6] Wang Q, Jing J Y and Wang B T 2019 *IEEE Trans. Instrum. Meas.* **68** 3350
[7] Bhardwaj H, Sumana G and Marquette C A 2020 *Food Chem.* **307** 125530
[8] Dong J, Zhang Y, Wang Y, Yang F and Chen Z 2019 *Opt. Express* **27** 11348
[9] Chen L, Liu B, Liu J, Wan S P and Wu Q 2020 *IEEE Sensors J.* 1
[10] Zhu Z, Liu L, Liu Z, Yu Z and Zhang Y 2017 *Opt. Lett.* **42** 1982
[11] Zhu Z, Liu L, Liu Z, Yu Z and Zhang Y 2017 *Opt. Lett.* **42** 2948
[12] Liu Z H, Liu W, Lai B, Zhang Y, Zhang Y X, Yang X H, Zhang J Z and Yuan L B 2021 *Opt. Express* **29** 18305
[13] Kurihara K, Ohkawa H, Iwasaki Y, Niwa O, Tobita T and Suzuki K 2004 *Anal. Chim. Acta* **523** 165
[14] Herrera N D, Esteban O, Navarrete M C, Gonzalez-Cano A, Benito-Pena E and Orellana G 2011 *Opt. Lasers Eng.* **49** 1065
[15] Coelho L, Almeida J M, Santos J L, Ferreira R A S, Andre P S and Viegas D 2013 *Fifth European Workshop on Optical Fibre Sensors*, May 19–22, Krakow, Poland
[16] Coelho L, Almeida J D, Moayyed H, Santos J L and Viegas D 2014 *J. Lightwave Technol.* **33** 432
[17] Iga M, Seki A and Watanabe K 2004 *Sensors Actuat. B-Chem.* **101** 368
[18] Goh L S, Kumekawa N, Watanabe K and Shinomiya N 2014 *Comput. Electron. Agr.* **101** 110
[19] Hosoki A, Nishiyama M, Sakurai N, Igawa H and Watanabe K 2020 *IEEE Sensors J.* **20** 227
[20] Lu M D, Peng W, Liu Q, Liu Y, Li L X, Liang Y Z and Masson J F 2017 *Opt. Express* **25** 8563
[21] Nasirifar R, Danaie M and Dideban A 2019 *Optik* **186** 194
[22] Wang Q, Wang X Z, Song H, Zhao W M and Jing J Y 2020 *Opt. Laser Technol.* **124** 106002
[23] Wei Y, Li L L, Liu C L, Su Y D, Zhao X L, Wu P, Hu J X, Wang R, Ran Z and Zhu D 2021 *Appl. Opt.* **60** 1366